Письма в ЭЧАЯ. А. 2012. Т. 9, № 8. С. 57–79

CHEMICAL COMPOSITION AND STRUCTURAL CHANGES OF Pd SAMPLE AND OF NOVEL SYNTHESIZED STRUCTURE UNDER γ-QUANTA IRRADIATION IN DENSE DEUTERIUM GAS

A. Yu. Didyk [a,1], *R. Wisniewski,* [b,2]

[a] Joint Institute for Nuclear Research, Dubna

[b] National Center of Nuclear Research (Narodove Centrum Badan Jadrowych), Otwock, Poland

Studies have been carried out into the element composition of Pd and brass with associated materials and of synthesized novel structure (ANNAWIT), placed in dense deuterium gas in a special high-pressure chamber (HPC) under the pressure of 3 kbar and irradiated with γ quanta of energy up to 8.8 MeV. Using the methods of scanning electron microscopy, microelement chemical analysis, and X-ray diffraction, it was determined that in the absence of all HPC-forming materials in the chamber volume and walls, the synthesized structure is largely composed of alumosilicates and Al and Si oxides with high content of Ti compounds as rutile TiO_2, $Pd_{1.5}D_2$. Considerable anomalies in the chemical composition were found both on the surface and at large depth in a Pd specimen. The entire Pd surface turned into a structure comprised of Pd clusters, Cu and Zn compounds, with a notable content of Mg, Al, S, Si, K, Ca, Ti, and Fe compounds. Results of evaluative calculations, including computation of the Q value, are presented for nuclear reactions produced in a saturated with deuterium Pd specimen and dense deuterium gas under the action of γ quanta, neutrons, and protons of energies up to $E_n + E_p \approx E\gamma - \Delta W$ MeV generated by deuteron fission. The obtained results can be explained by «collective effects» as chain reactions caused by deuteron fission induced by protons ($E_p > 3.39$ MeV) and neutrons ($E_n > 2.25$ MeV), as well as by thermonuclear synthesis of deuterium atoms elastically scattered by protons of energies up to $E_p < E\gamma - \Delta W$ MeV.

Представлены результаты исследований химического состава и структуры поверхности образца Pd и сопутствующих элементов из различных материалов, а также элементного состава впервые синтезированной структуры (ANNAWIT), находящихся в специальной камере (HPC) с высоким давлением газообразного дейтерия (около 3 кбар), после облучения потоком гамма-квантов с энергией 8,8 МэВ. С помощью метода сканирующей электронной микроскопии и микроэлементного анализа, а также метода рентгеноструктурного анализа показано, что радиационным способом синтезированная структура (ANNAWIT) представляет собой диэлектрик голубого цвета, в химический состав которого входят элементы Al, Si, Pd, O, C и Ti, ранее не присутствовавшие в химическом составе входящих в HPC элементов. Причем Ti содержится в виде рутила — TiO_2, а палладий в виде дейтерида палладия — $Pd_{1,5}D_2$. Также досконально исследованы значительные изменения химического состава исходного особо чистого палладия. В частности, на поверхности Pd-образца присутствуют кластеры, состоящие из «чистого» Pd, Cu и Zn, а также в значительных количествах сопутствующие элементы Mg, Al, S, Si, K, Ca, Ti и Fe. Кроме того, присутствуют Ru и Rh. Обсуждаются возможные феноменологические подходы, основанные на проведенном микроэлементном анализе, механизмы «горячего» D–D слияния, образования цепных реакций с умножением нейтронов и протонов, а также деления ядер средних масс.

PACS: 61.80.Cb

[1] E-mail: didyk@jinr.ru

[2] E-mail: roland.wisniewski@gmail.com

INTRODUCTION

Since the middle of the previous century and even earlier, there have been carried out studies of the processes taking place in deuterium and tritium plasma and of related activities on the construction of experimental thermonuclear reactors (TNR) [1–3]. In spite of the achieved progress, the problem of TNR creation still remains outstanding, although all the processes taking place in a TNR have been fairly well investigated [1, 2].

As is known, the cross section of deuteron photofission producing neutrons and protons is rather well studied while the corresponding cross sections of $D(\gamma, n)p$ reactions were measured experimentally [4, 5] and described theoretically fairly long ago [6]. At the maximal energy, the cross section of deuteron photofission reaches the value $\sigma_{\gamma,n}(E_\gamma = 4.4 \text{ MeV}) = 2.4$ b. The existing accelerators of electrons with energies up to 10 MeV and greater at electron fluxes up to several mA allow one to obtain high values of gamma-quanta fluxes on the targets [4].

In this paper, an alternative approach is considered for the use of deuterium photofission reactions produced in dense and superdense molecular deuterium gas under the action of bremsstrahlung. In each act of deuteron fission, a neutron and a proton are generated with energies defined by the reaction kinematics and energy–momentum conservation law.

The goal of this research is to study the neutron yield from dense molecular deuterium under the action of gamma quanta with energies lower than the characteristic energies of the giant dipole resonance ($E_\gamma < 10$ MeV) [4] and from palladium saturated with atomic deuterium, as well as to investigate processes of formation of new structures with different chemical compositions in possible nuclear and chemical synthesis reactions.

1. EXPERIMENTAL TECHNIQUE

In order to conduct this research, a specialized high-pressure chamber filled with deuterium (HPC) was designed and several modifications were fabricated. The principles of HPC construction are described in [7] (see also [8]). The scheme of the HPC with deuterium and Pd specimen inside, used in the experiment, is presented in Fig. 1.

Inside the HPC with an inner diameter of 4 mm there was placed a cylindrical Pd specimen (with 99.996% purity) of size $d_{\text{Pd}} = 3.8$ mm and length $L_{\text{Pd}} = 0.5$ cm (position *9* in Fig. 1). A distance manganin sleeve (with the common composition $\text{Cu}_{84}\text{Mn}_{14}\text{Ni}_2$) of length $L_{\text{CuMnNi}} = 5$ mm (position *10* in Fig. 1) was disposed between the Pd specimen and brass screw of length $L_{\text{CuZn}} = 0.5$ cm and diameter $d_{\text{CuZn}} = 0.4$ cm (position *12* in Fig. 1) with a «novel» chemical substance synthesized through nuclear-chemical reactions in the HPC (synthesized structure, position *11* in Fig. 1). This sleeve is meant to separate the metallic Pd specimen from the brass screw and simultaneously control small-size particles or complexes of atoms which escape from the Pd specimen or from the brass screw into the Pd specimen since evaporation processes take place according to the $\cos\Theta$ law, where the angle Θ is reckoned from the normal to the surface from which the atoms or atomic clusters evaporate. Pressure in the HPC was measured using strain gauge pressure sensor [7, 8] (position *14* in Fig. 1).

An experiment to study γ-quanta irradiation effects was carried out at the cyclic electron accelerator Microtron MT-25 with the maximum energy of electons up to 25 MeV in the Flerov Laboratory of Nuclear Reactions. The electron energy was chosen as $E_e = 9.3$ MeV

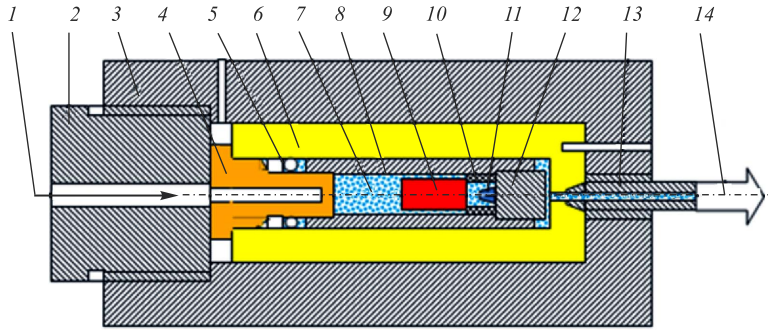

Fig. 1. The schematic drawing of high-pressure apparatus (High-Pressure Chamber — HPC). *1* — e^-, g, H^+, D^+ (or other chosen irradiating particles); *2* — closing screw with hole; *3* — reinforcing high-pressure chamber body; *4* — $CuBe_2$ «window» plug; *5* — high-pressure seals; *6* — $CuBe_2$ high-pressure chamber; *7* — (hydrogen) deuterium under high pressure; *8* — brass sleeve; *9* — investigated specimen (Pd); *10* — distance manganin sleeve; *11* — expected reaction product; *12* — brass screw; *13* — high-pressure connecting capillary; *14* — high-pressure valve, strain gauge pressure sensor and gas filling inlet

so that by using electrons of energies $E_e < 10$ MeV and, consequently, also bremsstrahlung of $E\gamma < 10$ MeV, one can exclude the giant dipole resonance influence at which energies ($10 < E\gamma < 30$ MeV) the cross section of (γ, n) reactions begins to grow up to 200–300 mb for medium mass nuclei [4, 9, 10].

The γ quanta was obtained on a tungsten target shaped as a 3-mm-thick W-plate using a 25-mm-thick aluminum electron absorber positioned behind it [11]. The beam dimensions on the braking target were 6–8 mm, with the measured angular divergence of the beam of γ quanta being approximately $8{-}10^0$ per 0.7 of angular distribution height [11].

The HPC inside volume $V_{\mathrm{D}} = 0.264$ cm^3. This is taken to mean the volume of a gas-filled chamber of length $L_{\mathrm{Al}} = 2.1$ cm and inner diameter $d = 0.4$ cm with a Pd-specimen of length $L_{\mathrm{Pd}} = 0.5$ cm and diameter $d_{\mathrm{Pd}} = 0.38$ cm disposed inside it and filled with atomic deuterium [7, 12] under the pressure $P = 3$ kbar. At such a pressure, the density of gaseous deuterium $\rho_{\mathrm{D}} \approx 0.1734$ g/cm^3 while its molecular density $n_{\mathrm{D}_2} = 2.593 \cdot 10^{22}$ mol. D_2/cm^3 (see [13]). Therefore, the overall number of deuterium atoms in the HPC inner volume was: $N_{\mathrm{D}} = 2N_{\mathrm{D}_2} = 2n_{\mathrm{D}_2} \cdot V_{\mathrm{D}} = n_{\mathrm{D}_2} \cdot V = 1.369 \cdot 10^{22}$ at. D. In order to evaluate the flux of γ quanta entering the HPC inner volume filled with deuterium and a Pd specimen, the coefficient β is introduced which allows for recalculation of the energy spectrum of γ quanta from the units of measurement in MeV$^{-1} \cdot$ sr^{-1} into the flux density of γ quanta in cm^{-2} and per area of the entrance window plug at the HPC target. In the calculations, the coefficient β is chosen from the maximally possible losses, i.e., from the minimal fluxes of γ quanta on the target, namely, $\beta = S_0/\Sigma_0 \approx 0.02$, where $S_0 = \pi d^2/4 = 0.126$ cm^2 is the HPC window plug area, $\Sigma_0 = \pi[L_{\mathrm{W}} + L_{\mathrm{Al}}]^2/4 = 6.158$ m^2.

Figure 2 shows cross sections of the deuteron photofission and energy spectrum of bremsstrahlung at $E_e < 8.8$ MeV and $\gamma < 23$ MeV. The energy dependence of the deuteron photodecay cross section from the reaction

$$\gamma(E_\gamma \geqslant \Delta W) + {}^2d^1 \rightarrow {}^1n^0 + {}^1p^0 \qquad (1)$$

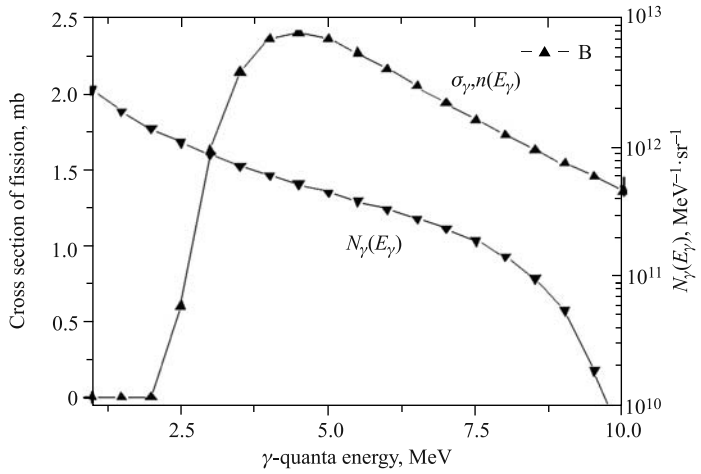

Fig. 2. Cross section of deuteron photodecay $\sigma_{d(\gamma,n)p}$ (mb) and spectrum of γ quanta $N_\gamma(E_\gamma)$ (MeV$^{-1}\cdot$sr^{-1}) versus energy

can be quite well described by the Bethe–Peierls formula [6, 4]:

$$\sigma_{d(\gamma,n)p} = \frac{8\pi}{3}\frac{e_0^2\hbar}{Mc_0}\sqrt{\Delta W}\,\frac{(E_\gamma - \Delta W)^{3/2}}{E_\gamma^3}, \tag{2}$$

where e_0, c_0, and M are the elementary charge, velocity of light, nucleon mass, and $\Delta W = 2.22$ MeV is the deuteron bond energy, respectively. In this case, reaction (1) yields a neutron and a proton with approximately equal energies, i.e., $E_n \approx E_p = 0.5[E_\gamma - \Delta W]$, since the momentum of γ quanta is small.

It is necessary to multiply expression (2) by the correction coefficient 1.7 for compliance of calculated and experimental values of cross sections [4]. The maximal cross section of the $d(\gamma, n)p$ reaction is reached at $_\gamma = 2\Delta W = 4.4$ MeV and makes up $\sigma^{\max}_{\mathrm{D}(\gamma,n)p} = 2.4$ mb (see Fig. 2). With the exception of the threshold region ($E_\gamma < 3$ MeV) and region above 100 MeV, the Bethe–Peierls formula fairly well describes the experimental dependence of the cross section of deuteron photodecay.

Figure 3 shows the cross section of the deuteron photodecay $\sigma_{d(\gamma,n)p}$ and energy spectrum of γ quanta at the electron beam current $J = 1$ μA ($6.25{\cdot}10^{12}$ e^-/s) and energy $E_e = 10$ MeV. The bremsstrahlung energy spectrum $N_\gamma(E_\gamma)$ was calculated using the expressions presented in [12, 13].

We now calculate the number of neutrons and protons produced at the passage of γ quanta with the maximal energy $E_\gamma < 8.789$ MeV (generated by electrons with the maximal energy $E_e = 9.3$ MeV at the electron current beam $J = 1$ μA) using the expression:

$$Y(E_y^{\max}) = \sum_{i=I_{\min}}^{i=I_{\max}} Y_i = \sum_{i=I_{\min}}^{i=I_{\max}} \beta N_{\mathrm{D}} \int\limits_{E_\gamma^i}^{E_\gamma^{i+1}} \sigma_{d(\gamma,n)p}[E_\gamma] N_\gamma[E_\gamma]\, dE_\gamma, \tag{3}$$

where $E_\gamma^{I_{\min}} = \Delta W, E_\gamma^{I_{\max}} = E_\gamma^{\max} = 9.22$ MeV while $E_\gamma^i = (i-1)\Delta E_\gamma + \Delta W$, where $i = 1, 2, \ldots, 8$, $I_{\max} = (9.22 - \Delta W)/\Delta = 7$ at $\Delta E = 1$ MeV.

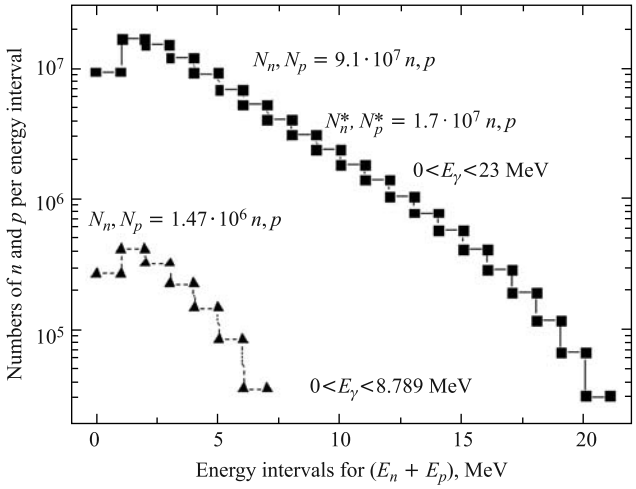

Fig. 3. Histograms with the number of neutrons and protons in 7 energy ranges (at $E_\gamma^{\max} = 9.3$ MeV) and 21 energy ranges (at $E_\gamma^{\max} = 23$ MeV), respectively, from reaction (1)

Figure 3 shows hystograms with the number of neutrons and protons in 7 (at $E_\gamma^{\max} = 9.3$ MeV) and 21 energy ranges ($E_\gamma^{\max} = 23$ MeV) from reaction (1), using (2) and (3), at the electron current on the braking target $J = 1$ μA. Neutron and proton yields $N_n(E_\gamma)$ and $N_p(E_\gamma)$, respectively, are also presented for two energies of electron beams of 1 μA.

The time of HPC exposure to γ quanta is $T \approx 2.22 \cdot 10^4$ s at the average current of the electron beam on the braking W-target $\bar{I}_{e^-} \approx 7$ μA (i.e., the average number of electrons $\bar{N}_{e^-} \cong 4.375 \cdot 10^{13}$ e^-/s). In the course of irradiation, measurement of the neutron flux near the HPC was done hourly for different geometric positions of the boron-based solid-state neutron detector [14]. During the neutron yield measurement, the distance and angular position of the detector were changed in respect to the irradiated target and HPC. Changes in the neutron flux were not observed for different positions of the neutron detector to the right and left of the HPC in the horizontal plane at the distance $L = 29$ cm, except for its position along the axis of the electron beam immediately behind the HPC (see Fig. 4).

Table 1 shows neutron radiation yields versus the electron beam current in presence of the HPC between the detector and aluminum absorber and in its absence. The measurement time is 30 s.

As one can see, the HPC with deuterium and palladium saturated with deuterium either a) intensively slows down neutrons which enter into a reaction inside the chamber and its walls without going out, or b) absorbs and moderates neutrons, leading to a decrease in the efficiency of registration by a neutron detector combined with a neutron moderator.

It should be also noted that during the irradiation by γ quanta, the HPC was cooled by a flux of compressed air at the temperature $\approx 20\,^\circ$C, nevertheless, the temperature of the HPC external surface significantly exceeded $100\,^\circ$C even though temperature measurements were not undertaken.

Prior to opening the HPC, its pressure was measured to be $P = 3$ kbar and some hold-up time aimed to decrease induced activity was allowed to elapse before the chamber was finally opened. The palladium specimen (Fig. 1, position *9*) with the external initial diameter

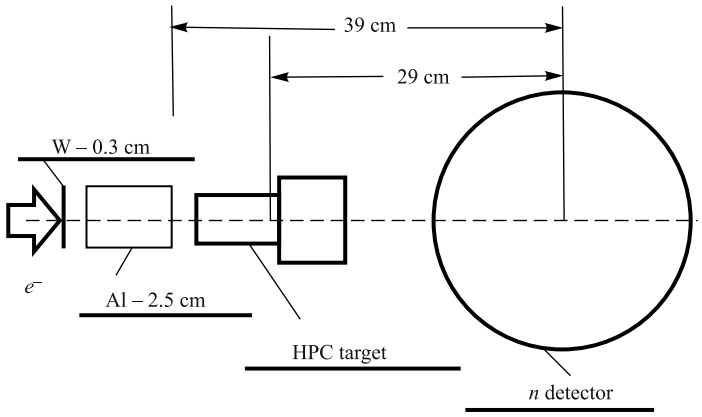

Fig. 4. The scheme of braking W-target, Al-absorber, high-pressure chamber (HPC), and neutron detector with a moderator during neutron yield measurements

Table 1. **Neutron yield from the electron beam current with positioned HPC (as shown in Fig. 2) and without it**

Position of HPC	Electron beam		
	1 μA	4 μA	7 μA
Without HPC, μSv/h	350 ± 19	577 ± 24	898 ± 30
With HPC, μSv/h	310 ± 16	462 ± 21	628 ± 25
Relation	0.89	0.80	0.70

$d_{\mathrm{Pd}} = 3.8$ mm was found to be wedged due to its increased overall dimensions inside the brass sleeve (Fig. 1, position *9*) with the inside diameter $d = 4$ mm. Approximately in 2–3 days the palladium specimen decreased in size and was easily extracted.

2. RESULTS OF STRUCTURAL-PHASE AND ELEMENT ANALYSIS OF ALL HPC COMPONENTS FOUND IN THE INSIDE VOLUME FILLED WITH GASEOUS DEUTERIUM

It is important to mention that the X-ray and microelement zond analyses and surface studies were carried out at three independent scientific centers using different electronic scanning microscopes as: Zeiss Evo 40 scanning electron microscope equipped with an X Flash 1106 silicon drift detector (SDD), JEOL JSM-5910LV scanning electron microscope with an Oxford Instruments INCA ENERGY analysis system, D8 DISCOVER diffractometer with GADDS (CuK_α radiation with a graphite monochromator). We now present separately the results of the study into the structure and chemical composition of *all the components* (see Fig. 1) with the surfaces facing inside of the HPC.

2.1. Synthesized Novel Structure (SNS). On the flat inside surface of the brass screw (Fig. 1, position *12*), *as had been expected*, there was discovered a synthesized novel structure (SNS), formed due to the action of γ quanta on the dense deuterium gas and materials placed

in the HPC. The optical and electron-microscopy (SEM) images of this structure are presented in Fig. 5. It is significant that the SNS structure proved to be dielectric with a high value of dielectric permeability ε, therefore, in order to allow electron-microscopy studies the surfaces of the SNS structure and brass screw were covered with a thin gold layer of thickness up to 1000 Å (see Fig. 5, *b*). The initial colour of the SNS structure was blue (see Fig. 5, *a*) but changed to a darker one after coating.

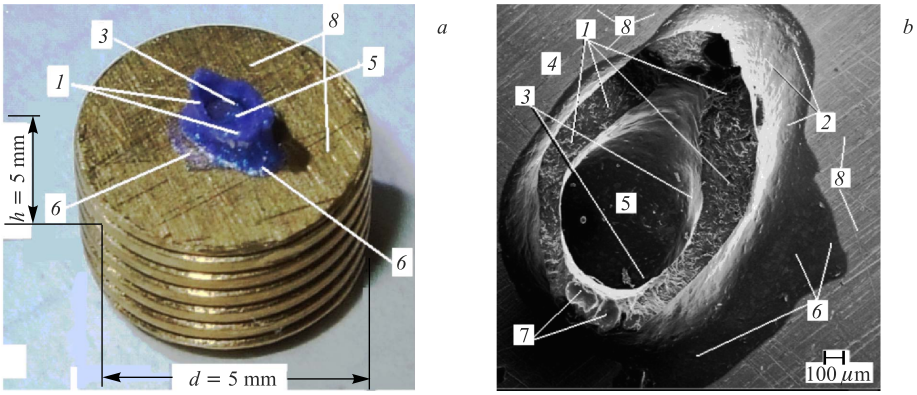

Fig. 5. *a*) A photo of the brass screw (Fig. 1, position *12*) with the synthesized novel structure (SNS) and *b*) image with the structure made by scanning electron microscopy (top view). The following designations are used in the photos: *1* — upper part of walls of «volcanic» structure with «crater»; *2* — shallow walls of SNS; *3* — smooth side walls of «crater»; *4* — brass screw surface; *5* — «crater» floor with structures of various compositions; *6* — molten and spread over surface «lava» from «crater»; *7* — molten and hardened clusters of SNS material; *8* — brass screw surface

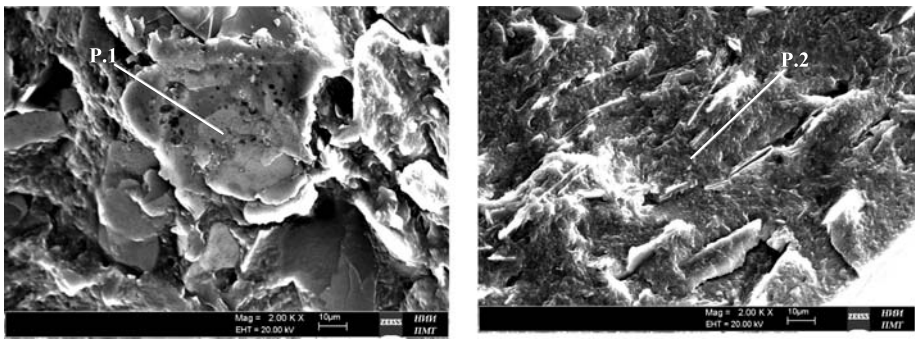

Fig. 6. Microstructure of two patches of the upper flat area around the «crater»

Figure 6 shows SEM images of SNS patches on the flat top. The chemical composition of these patches is given in Table 2. Further we present SEM images of surfaces of all objects studied by scanning electron microscopy and X-ray microanalysis at the points marked in each SEM image.

Table 2. **Concentrations of chemical elements, obtained by microelement analysis from the surface in Fig. 6 at marked points 1 and 2**

Element	Z	X-ray series	C_W, wt. %	Error, wt. %	C_A, at. %
Carbon, C	6	K-series	25.08	3.42	40.24
Oxygen, O	8	K-series	35.60	4.43	42.87
Sodium, Na	11	K-series	0.78	0.08	0.65
Magnesium, Mg	12	K-series	1.77	0.12	1.40
Aluminum, Al	13	K-series	4.88	0.25	3.49
Silicon, Si	14	K-series	5.41	0.24	3.71
Potassium, K	19	K-series	1.51	0.07	0.75
Titanium, Ti	22	K-series	13.07	0.37	5.26
Copper, Cu	29	K-series	1.44	0.09	0.44
Zinc, Zn	30	K-series	0.87	0.07	0.26
Gold, Au	79	L-series	9.60	0.37	0.94
Total			100.0		100.0

It should be noted that in the measured area on the «crater» top there was observed a significant amount of such elements as Ti (13.07 wt. %), Al (4.88 wt. %), Si (5.41 wt. %), Mg (1.77 wt. %) and very small amount of basic elements Cu (1.44 wt. %) and Zn (0.87 wt. %) which form the basis of the brass screw.

Shown in Fig. 7 is SEM microstructure of the virgin brass (*a*) and surface of the brass screw (*b*) near the SNS (see Fig. 1, position *12*).

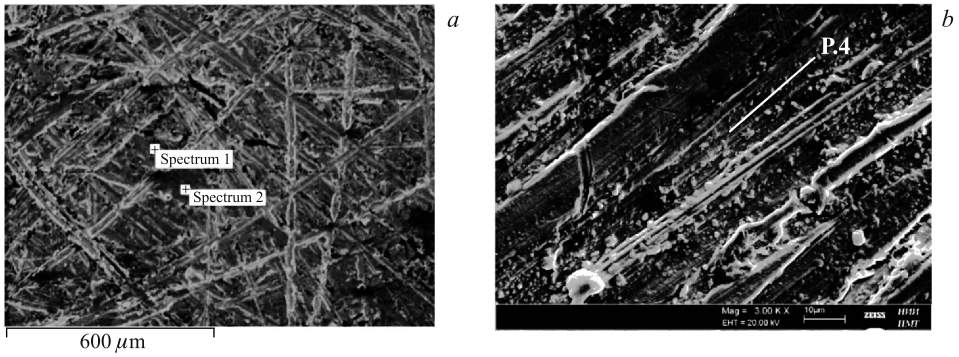

Fig. 7. Microstructure of virgin brass (*a*) and surface of the brass screw (*b*) around the SNS structure

Figure 8 presents an image of surface patch on the boundary between the spread «lava» from the «crater» and patch of the outwardly normal looking brass screw. Tables 3 and 4 provide the element composition of the analyzed surface patches (p. 5) and (p. 6), respectively.

Note that on the measured patches of the brass screw one can observe elements which are bound to be there, except for iron and niobium.

All the elements observed on the flat top of the «volcano with a crater at the centre» structure were present on the molten patch or the so-called lava, although in changed quantities:

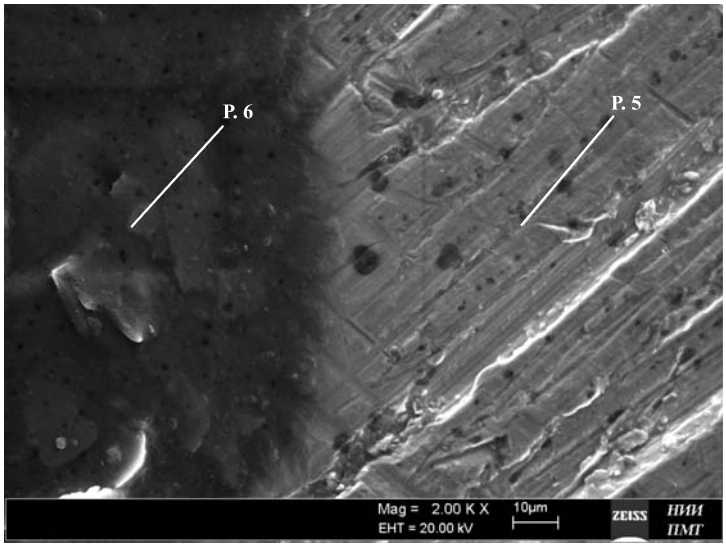

Point 6 Point 5

Fig. 8. Microstructure on the boundary between the melt and brass screw (see Fig. 5, positions *6* and *8*)

Table 3. **Concentrations of chemical elements obtained by microelement analysis from the surface in Fig. 8 at marked point 5**

Element	Z	X-ray series	C_W, wt. %	Error, wt. %	C_A, at. %
Carbon, C	6	K-series	10.98	2.29	39.70
Oxygen, O	8	K-series	4.00	0.85	10.86
Copper, Cu	29	K-series	42.87	1.22	29.29
Zinc, Zn	30	K-series	27.70	0.84	18.40
Niobium, Nb	41	L-series	3.19	0.16	1.49
Iron, Fe	26	K-series	0.33	0.05	0.25
Total			100.0		100.0

Table 4. **Concentrations of chemical elements gained by microelement analysis from the surface in Fig. 8 at marked point 6 (in the spread melt near the SNS)**

Element	Z	X-ray series	C_W, wt. %	Error, wt. %	C_A, at. %
Carbon, C	6	K-series	37.09	4.66	55.01
Oxygen, O	8	K-series	31.51	4.01	35.08
Magnesium, Mg	12	K-series	2.02	0.13	1.48
Aluminum, Al	13	K-series	1.39	0.09	0.92
Silicon, Si	14	K-series	3.56	0.15	2.26
Potassium, K	19	K-series	0.77	0.06	0.35
Titanium, Ti	22	K-series	6.54	0.20	2.47
Copper, Cu	29	K-series	3.05	0.16	0.85
Zinc, Zn	30	K-series	1.78	0.12	0.49
Gold, Au	79	L-series	12.21	0.51	1.10
Total			100.0		100.0

Ti (4.44 wt. %), Al (1.04 wt. %), Si (2.65 wt. %), Mg (1.77 wt. %) and higher concentrations of Cu and Zn which form the basis of the brass screw, i.e., Cu (2.26 wt. %), Zn (1.32 wt. %). This can be explained by that the spread layer is thin and the electron beam partially reaches the brass substrate during the analysis.

Figure 9 shows the «crater» structure with smooth walls and even edge shaped as an ellipsis with a large axis $b = 1.1$ mm and small axis $a = 0.82$ mm (*a*) as well as part of the «crater» wall with molten patches (*b*). On the «crater» floor one can observe microstructures which are practically not connected with the «crater» floor as they can move around on specimen rotation when viewing.

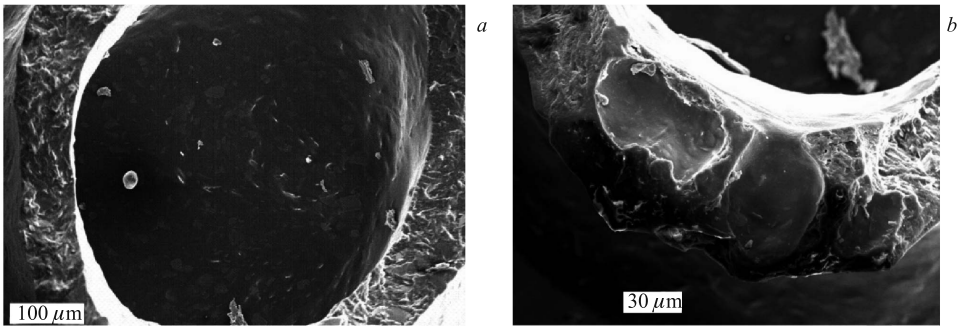

Fig. 9. Image of the «crater» with smooth walls and even edge (*a*) and patch of the «crater» wall with molten and congealed drops (*b*)

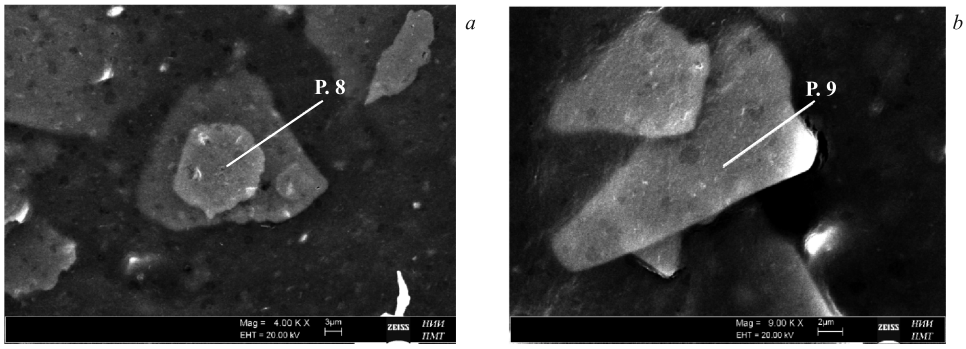

Fig. 10. Two SEM images of planar plate-like microstructures on the «crater» floor

Figure 10 presents planar plate-like structures located on the «crater» floor. The element composition of these structures is given in Table 5. It should be noted that the «crater» floor itself has the same chemical composition as these isolated, floor-covering plate-like structures.

As can be seen, on the «crater» floor one observes along with the smaller sphere-like structures also complex structures (SEM image in Fig. 11) and multiple plate-like structures of size 5–10 μm. The plate-like structures, according to Table 5, comprise large quantities of Ti ((66.42 ± 0.97) wt. %) contained as rutile (TiO_2) and its derivatives, as was shown by

Table 5. **Concentrations of chemical elements obtained by microelement analysis from the surfaces of plate-like structures in Fig. 10 at marked points (8 and 9) on the «volcanic crater» floor**

Element	Z	X-ray series	C_W, wt. %	Error, wt. %	C_A, at.%
Carbon, C	6	K-series	6.44	1.15	19.57
Oxygen, O	8	K-series	8.89	1.56	20.29
Potassium, K	19	K-series	4.26	0.16	3.98
Titanium, Ti	22	K-series	66.42	0.97	50.65
Iron, Fe	26	K-series	1.17	0.07	0.77
Copper, Cu	29	K-series	3.68	0.12	2.11
Zinc, Zn	30	K-series	2.54	0.10	1.42
Gold, Au	79	L-series	6.59	0.23	1.22
Total			100.0		100.0

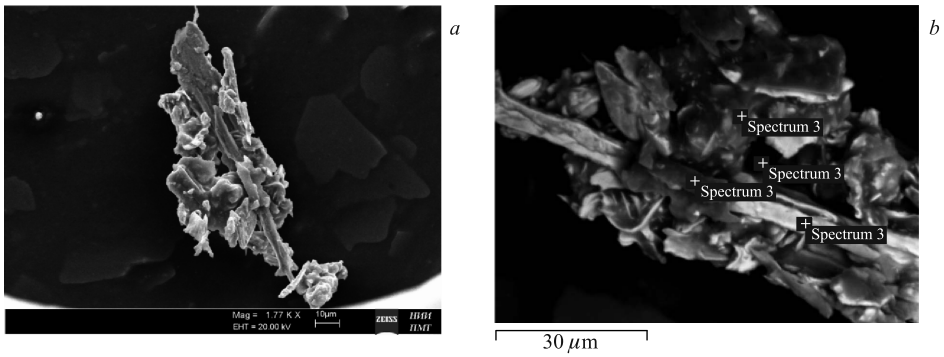

Fig. 11. *a*) Complex microstructure on the «crater» floor, largely composed of brass. *b*) SEM image of recrystallized complex structure largely composed of brass (Cu, Zn)

X-ray analysis. It should be noted that on the measured patches of the «crater» top there was observed a substantial amount of K ((4.26 ± 0.16) wt. %), which is close in nucleus charge to titanium, and Fe ((1.17 ± 0.07) wt. %), as well as small quantities of Cu ((3.68 ± 0.12) wt. %) and Zn ((2.54 ± 0.10) wt. %). The copper and zinc concentrations in the plate-like structures can be compared to their concentrations on top of the SNS «crater» walls (Table 2) and in the alloy on the brass screw surface (Table 4).

Figure 11 shows a SEM image of the complex recrystallized structure from the crater floor of the synthesized structure (SNS).

Figures. 11, *a, b* and 12 show SEM images of two more structures observed on the crater floor with microelement analysis spectra at the indicated points. The spectrum taken at point 4 (Spectrum 4) via the opening through which the «crater» floor can be viewed indicates presence of titanium (Ti). The chemical composition at the other three points of recrystallized structure corresponds to brass with small inclusions of other elements, in places absolutely without titanium.

Figure 13 shows a SEM image of the upper flat part of «crater» walls. The element composition for each measured point (Spectra 1–4) is given in Table 6.

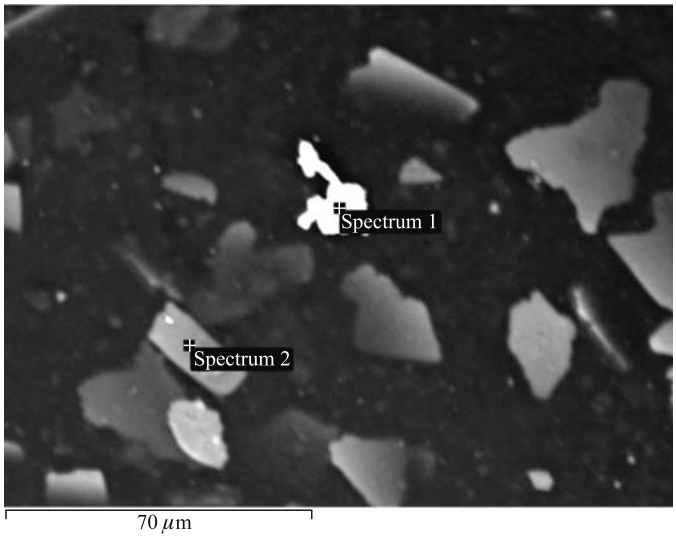

Fig. 12. SEM image taken using the reflected neutron method and presenting a white complex structure largely composed of palladium as well as multiple plate-like structures

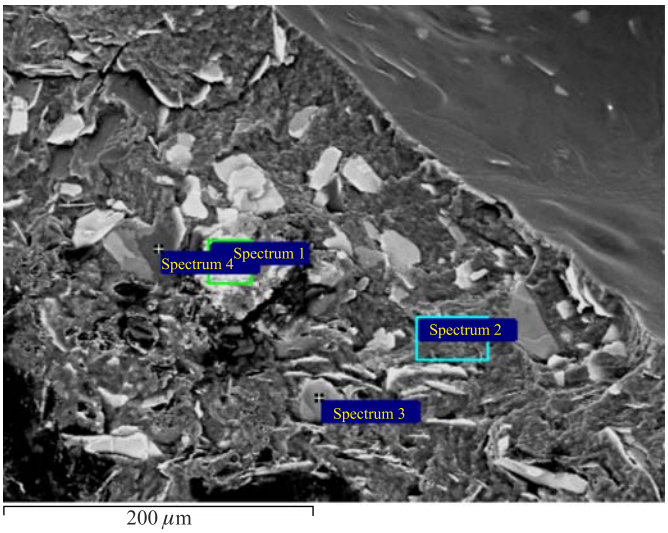

Fig. 13. SEM photo of the flat top of SNS «crater»

Table 6. **Element composition (wt. %) at all four measured points (Spectra 1–4)**

Number	C	O	Mg	Al	Si	Cl	K	Ca	Ti	Fe	Cu	Zn	Au
Spectrum 1	26.81	37.78	0.44	5.27	6.88	—	1.7	0.31	13.17	0.31	1.17	0.67	5.49
Spectrum 2	50.5	38.43	1.62	—	2.92	—	—		0.32	—	—	0.81	5.39
Spectrum 3	38.51	26.35	0.74	4.81	7.36	0.27	1.76		9.73	—	0.7	0.83	8.93
Spectrum 4	56.69	30.39	1.7	0.89	4.03	—	0.28		2.54	—	—	0.67	2.81

As one can see, at two measured points the high concentration of Ti (13/17 and 9.73 wt. %) is accompanied by inclusion of associated elements as Al (5.27 and 4.81 wt. %), Si (6.88 and 7.36 wt. %), and K (1.7 and 1.76 wt. %) and also such elements as Fe, Ca, Cl, and Mg. Figure 14 shows a SEM image of the brass screw surface containing congealed «lava from the crater» together with the chemical composition measured at six points from the right edge of the brass screw towards the melt. In Tables 7 and 8, the element composition is presented for six points from one side (Spectra 1–6) and for four points from the other side of the SNS synthesized structure, i.e., along the diameter.

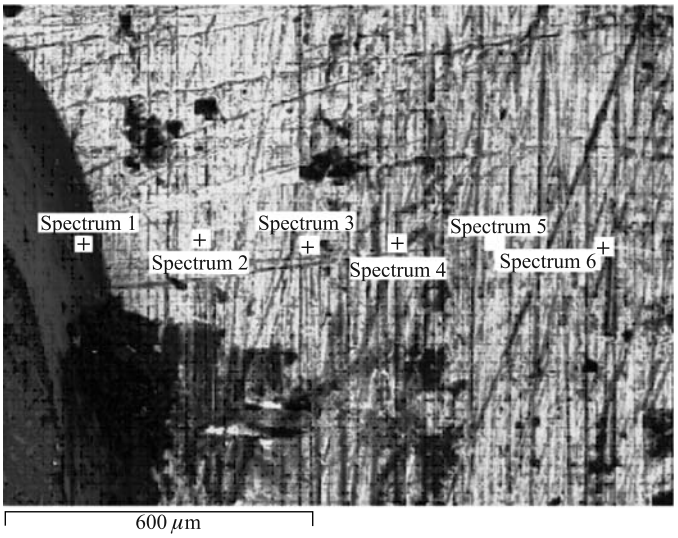

Fig. 14. SEM image of the brass screw with melt spread near the SNS

Table 7. **Element composition at all analyzed points 1–6 (Spectra 1–6) on the surface of the brass screw from one side of the SNS structure**

Number	C	O	Na	Mg	Al	Si	Cl	K	Ca	Ti	Fe	Cu	Zn	Pd	Au	Cu/Zn
Spectrum 1	40.21	25.79	—	1.58	0.33	3.46	—	0.87	0.26	12.88	0.46	3.6	2.49	0.99	7.07	—
Spectrum 2	28.73	2.47	—	—	—	—	0.12	—	—	—	0.19	38.84	25.45	—	4.21	1.52613
Spectrum 3	31.79	1.12	—	—	—	—	—	—	—	—	0.25	41.59	24.76	—	0.48	1.679725
Spectrum 4	49.81	7.43	0.72	—	0.37	—	0.45	—	0.17	0.28	0.86	21.45	12.98	—	5.47	1.652542
Spectrum 5	33.16	2.12	—	—	0.17	0.13	—	—	0.26	—	0.2	39.97	23.29	—	0.7	1.716187
Spectrum 6	39.78	6.16	—	—	1.06	0.86	—	—	—	0.12	0.15	29.74	17.39	—	4.72	1.710178

Table 8. **Element composition at all analyzed points 1–4 (Spectra 1–4) on the surface of the brass screw from one side of the SNS structure**

Number	C	O	Al	Si	Fe	Cu	Zn	Pb	Total	Cu/Zn
Spectrum 1	42.68	6	0.26			30.64	20.43		100	1.499755
Spectrum 2	46.96	5.62	0.26		0.47	27.96	16.53	2.21	100	1.69147
Spectrum 3	49.33	7.21	0.53	0.24		27.57	15.12		100	1.823413
Spectrum 4	44.5	6.68	0.48	0.31		30.36	17.69		100	1.716224

As is evident from Tables 7 and 8, an almost systematic increase in the copper concentration to zinc ratio can be observed closer to the brass screw edge.

Figure 15 presents a SEM photo of the virgin brass used for fabrication of the brass screw and irradiated surface (see Fig. 1, position *12*). Element compositions for two points on the surface of the virgin brass (Spectra 1, 2) are given in Table 9. Basing on a comparison of chemical element compositions of the brass and virgin brass surfaces irradiated by γ quanta, one can make the following conclusions. The virgin brass contains almost only copper (52.64 and 55.45 wt. %) and zinc (33.04 and 33.28 wt. %), including also Al (3.12 and 3.39 wt. %) and Fe (0.42 and 0.46 wt. %) with relatively small concentrations of carbon (7.99 and 11.27 wt. %) and oxygen (2.8 wt. %). In the irradiated brass the relative concentrations of copper and zinc decreased significantly: up to less than 40 wt. % for Cu and up to 25 wt. % and less for Zn. The aluminum $^{27}\mathrm{Al}^{13}$ concentration also decreased, however, there was produced silicon, most likely $^{28}\mathrm{Si}^{14}$ isotope, which could be formed in the reaction $n + {}^{27}\mathrm{Al}^{13} \to \gamma + {}^{28}\mathrm{Si}^{14}$ with the Q — value equal to 12.368 MeV.

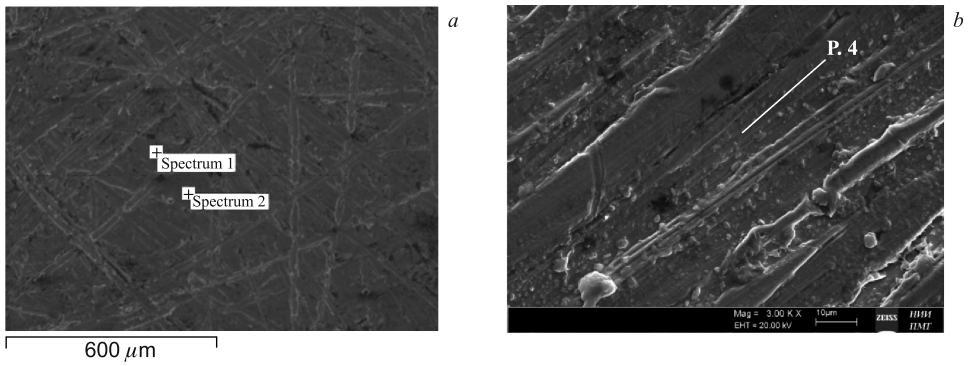

Fig. 15. *a*) SEM image of the virgin brass from which the brass screw is fabricated and *b*) surface of the brass screw near the SNS structure

Table 9. **Element compositions at two analyzed points 1 and 2 (Spectra 1, 2) in wt. %. The normalized element composition minus carbon is given in the same table in the two bottom lines**

Number	C	O	Al	Fe	Cu	Zn	Cu/Zn	Total
Spectrum 1	7.99	2.8	3.12	0.42	52.64	33.04	1.59322	100
Spectrum 2	11.27	—	—	—	55.45	33.28	1.67473	100
Spectrum 1	—	3.04	3.39	0.46	57.21	35.91	1.593150	100
Spectrum 2	—	—	—	—	62.49	37.51	1.665956	100

The brass surface was irradiated by γ quanta (Fig. 14 gives the impression of deeper scratches than on the virgin brass (Fig. 15).

2.2. Microstructure and Element Composition of Split Manganin Foil (Fig. 1, Position *10* — Distance Manganin Sleeve). Figure 16 shows SEM images from the side facing inside the HPC chamber (*a*) and from the other side of the split separating foil (see Fig. 1, position *10*). The element compositions on the inner and external sides of the foil are given in Table 10, where the spectra above 1–3 refer to (*a*) and the spectra below 4–6 correspond to (*b*).

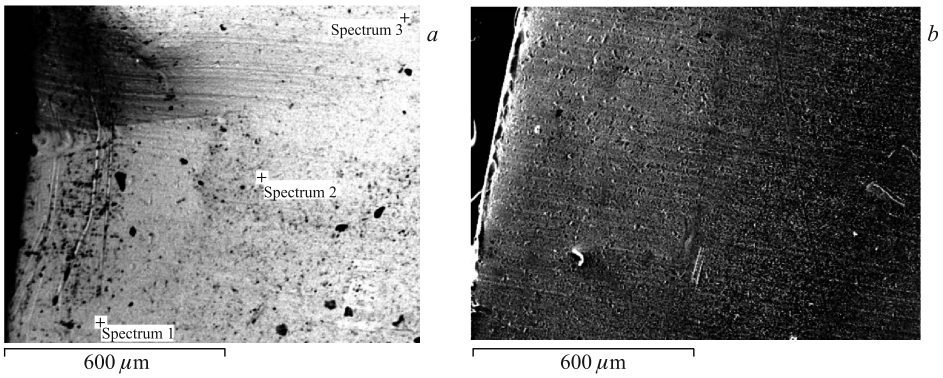

Fig. 16. SEM image of the split separating foil from the side facing inside the chamber (*a*) and the other side (*b*) adjacent to the loading brass screw

Table 10. **Element compositions from two sides of separating manganin foil**

Points	C	O	Mn	Ni	Cu
Inner side					
Spectrum 1	11.38	0.96	10.10	2.60	74.96
Spectrum 2	10.86	1.08	10.06	2.80	75.20
Spectrum 3	10.76	1.68	10.03	2.85	74.68
External side					
Spectrum 4	12.75	—	10.36	2.92	73.97
Spectrum 5	16.93	1.50	9.34	2.83	69.40
Spectrum 6	8.71	1.53	10.23	2.96	76.57
Systematics of measurements					
Mean	11.00	1.24	10.06	2.75	74.95
Std. Deviation	0.33	0.39	0.04	0.13	0.26
Max.	11.38	1.68	10.10	2.85	75.20
Min.	10.76	0.96	10.03	2.60	74.68

The virgin material of the split separating manganin foil has a commonly used composition $Cu_{84}Mn_{14}Ni_2$.

As one can see, the inner surface of the split separating manganin foil is free from such chemical elements as Zn, Ti, Si, K, Mg, S, and Al, which were found both in the synthesized SNS structure and in the Pd specimen. The ratio Cu:Mn for the external side is 7.33; 7.43; 7.30, while for the inner side it is 7.42; 7.46; 7.45. Therefore, no changes are observed in the copper concentration!

The most important conclusion one can make from the studies into the surface composition of the split separating manganin foil is as follows: *On the foil surface* only those elements are found which are bound to be in manganin! *The inner side, in its turn, is entirely* free from the chemical elements which are observed on the surface of the brass screw and, as is clear from the next section, of the Pd specimen.

This experimental fact testifies that no evaporative processes took place on the SNS surface with subtraction of substance, according to the $(\cos\theta)$ law, to the nearest surface of the Pd specimen and there were no reverse evaporative processes also.

At the same time, one must not rule out high-speed and targeted (at the angles close to the surface normal) subtraction of substance from the Pd surface to SNS structure surface, to brass substrate and conversely.

2.3. Surface Structure and Element Composition of Palladium Specimen. In Fig. 17, *a*, a SEM image of the cylindrical end surface of the virgin Pd specimen is presented. Figure 17, *b* provides an image of the Pd end surface closest to the SNS structure with criss-crossed, as above, points where microelement analysis was made.

Tables 11 and 12 display data from the element analysis of the virgin Pd and Pd irradiated by γ quanta, respectively. In these tables the element concentrations are given for the points marked in the corresponding Fig. 16, *a* and *b*.

For contrast sake, Fig. 17, *a, b* provides two SEM images made using the reflected electron method (Z contrast) with criss-crossed points to mark the spots where the element composition was determined. Therefore, the lighter spots correspond to greater values of atomic number of chemical elements. Tables 12 and 13 display element compositions for Fig. 18, *a* and *b*, respectively.

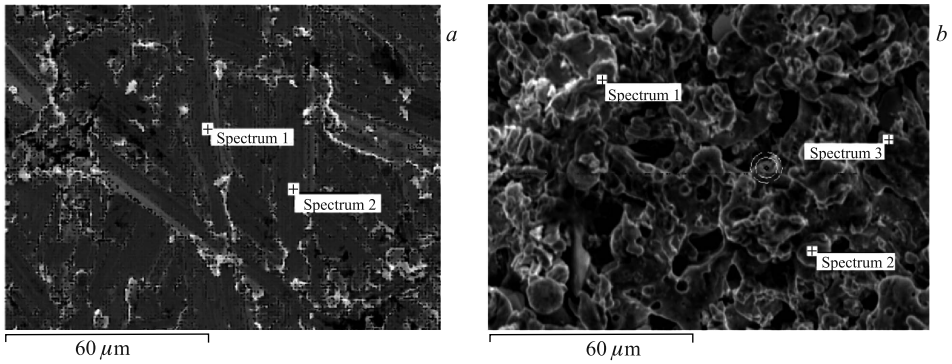

Fig. 17. SEM images of the ends of virgin (*a*) and irradiated by γ quanta (*b*) palladium specimens

Table 11. **Element compositions at three analyzed points 1–3 (Spectra 1–3) for grey (1), light (2) and dark (3) contrasts on the end surface of Pd specimen for Fig. 15, *a* in wt. %**

Number	O	Si	S	Ca	Ti	Cu	Zn	Pd	Total
Spectrum 1	3.05	—	—	—	—	49.25	37.99	1.51	100
Spectrum 2	—	—	—	—	—	12.55	5.92	74.26	100
Spectrum 3	14.64	0.65	1.08	0.71	1.38	8.29	3.81	25.66	100

Table 12. **Element compositions at four analyzed points 1–4 (Spectra 1–4) for light (1), lighter (2), grey (3) and less grey (4) colours on the end surface of Pd specimen in Fig. 18, *b* in wt. %**

Number	O	Mg	Al	Si	K	Ti	Cu	Zn	Pd	Total
Spectrum 1	—	—	—	—	—	—	6.45	3.02	88.18	100
Spectrum 2	—	—	—	—	—	—	3.88	2.55	93.58	100
Spectrum 3	22.76	—	3.37	3.4	0.54	11.61	31.20	10.41	10.71	100
Spectrum 4	2.89	0.38	—	—	—	—	28.73	7.59	52.49	100

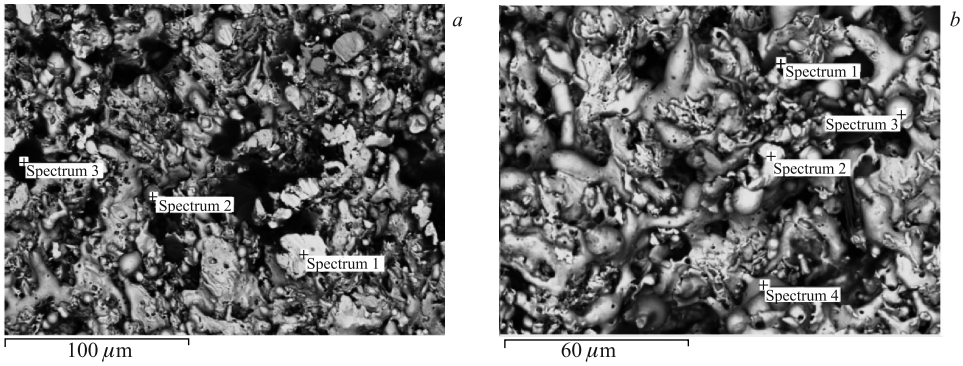

Fig. 18. SEM images of palladium specimen irradiated by γ quanta

The entire palladium structure turned into an inhomogeneous one, composed of separate clusters with different element compositions. That is precisely why it was impossible to remove the Pd specimen right upon opening the HPC chamber when this specimen had significantly grown in volume. Furthermore, there was no the so-called material swelling due to formation and clusterization of point radiation defects of Frenkel pairs — crystal lattice vacancies and atoms at interstitial positions. Such clusterization leads to creation of gas-filled pores or bubbles and extensive defects as interstitial loops, whereas swelling is reached at the temperatures exceeding 0.3 of the material's melting temperature. In the above case, palladium temperature was such that it enabled processes which brought about formation in some places of copper and zinc concentrations of up to 31.2 and 10.41 wt. % (point 3, Table 10) and 49.25 and 37.99 wt. % (point 1, Table 11). At the same time, the concentration of titanium was 1.38 wt. % and in some places proved to be up to 11.61 wt. % (point 3, Table 15) while for the associated elements (see Table 11, point 3) it was as follows: Si — 0.65 wt. %, S — 1.08 wt. %, Ca — 0.71 wt. % (see Table 12, point 3), as well as for other observed elements: Al — 3.37 wt. %, Si — 3.4 wt. %, K — 0.54 wt. %.

Table 13. **Element compositions in the cylinder side surface of irradiated palladium specimens in wt. %**

Irradiated end	C	O	Pd
Spectrum 1	27.81	12.93	59.26
Spectrum 2	19.82	—	80.18
Spectrum 3	18.27	35.67	46.07

Such phenomenal changes in the palladium composition and structure took place only due to the presence of high temperatures significantly exceeding the melting and, possibly, evaporating temperatures of palladium! These temperatures in their turn could be and *were caused by Pd nuclear fission reactions* with considerable temperatures as a result of energy release in individual nuclear fission acts.

In order to substantiate the above conclusion, we present images of surface structure of Pd specimens from the cylinder side surface (Fig. 19) and from the opposite end (Fig. 19), i.e., the nearest end to the place of penetration of γ quanta into the Pd specimen. All the images are given in pairs: virgin (*a*) and irradiated ones (*b*). Measured element concentrations on separate patches are summarized in Table 14 (Fig. 19) and Table 15 (Fig. 20).

As is obvious, considerable changes took place on the irradiated end of the Pd specimen. The side surface structure of the irradiated Pd specimen underwent dramatic changes whereafter the specimen acquired darker colour in comparison with the virgin specimen. The

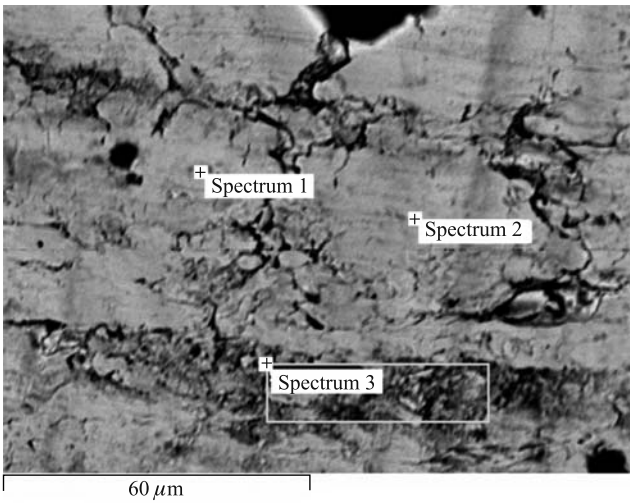

Fig. 19. SEM image of side surface irradiated by γ quanta Pd specimens. As before, microelement analysis is done at the marked points

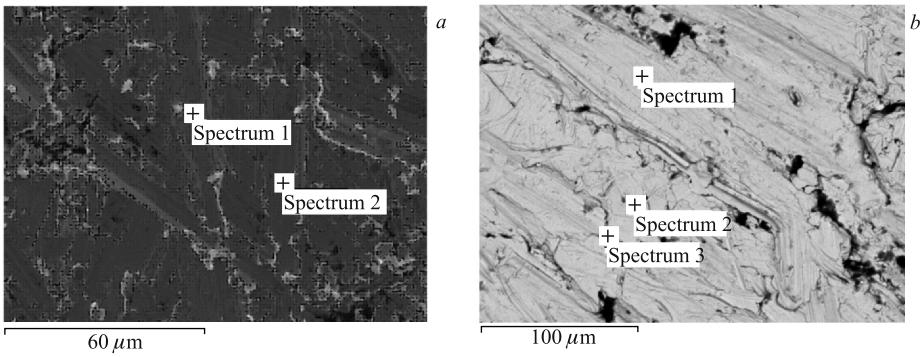

Fig. 20. SEM images of side surfaces of virgin (*a*) and irradiated by γ quanta (*b*) Pd specimens

Table 14. **Element compositions of the virgin (Fig. 20, *a*) and irradiated ends (Fig. 20, *b*) of the Pd specimen, the furthest from the SNS structure, i.e., at the place of entry of γ quanta, in wt. %**

Irradiated end	C	O	V	Cr	Fe	Pd	W
Spectrum 1	5.78	—	—	—	—	94.22	—
Spectrum 2	4.19	3	—	—	—	92.81	—
Spectrum 3	—	5.84	1.93	4.88	72.44	—	14.92

structure and surfaces of the bulky material became inhomogeneous, with multiple cracks and of darker contrast than in the areas with high palladium concentration. Apparently, in one of such cracks, which is also typical of other cavities and cracks of darker contrast, there were observed such elements as V^{23}, Cr^{24}, and Fe^{26}, Ru^{42}, Rh^{43}, W^{74}, Pt^{78}, Pb^{82}.

Table 15. **Element compositions on three segments of the dissected brass sleeve**

Number	C	O	Fe	Cu	Zn	Ta	Pb	Total
Fig. 21, *a*								
Spectrum 1	5.33	—	—	56.83	37.84	—	—	100
Spectrum 2	3.61	—	—	57.18	39.21	—	—	100
Spectrum 3	5.63	—	—	52.43	39.37	—	2.57	100
Fig. 21, *b*								
Spectrum 1	8.41	2.56	0.56	48.93	39.54	—	—	100
Spectrum 2	5.35	2.45	—	51.3	38.93	—	1.96	100
Spectrum 3	7.53	3.71	—	49.8	35.32	0.08	3.56	100
Spectrum 4	7.94	2.75	—	49.06	36.61	0.05	3.58	100
Another area								
Spectrum 1	8.19	—	—	51.91	39.9	—	—	100
Spectrum 2	13.67	2.97	—	44.82	32.35	—	6.19	100
Spectrum 3	10.86	3.77	—	49.68	35.69	—	—	100

As will be shown in the conclusions and discussions below, formation of impurities attests to presence in palladium of nuclear fission reactions whereby heavier Pd^{46} nuclei split into two lighter fragments as Ti^{22} and Cr^{24} and their derivatives.

2.4. Structure and Element Composition of Brass Sleeve (Fig. 1, Position *8* — Brass Sleeve). The last element to contact with the inside volume of the HPC chamber and dense gaseous deuterium was the brass sleeve, which was closed from the side whence the flux of γ quanta entered by an entrance plug 2 mm thick (the so-called window plug made of beryllium bronze) (Fig. 1, position *4* — $Cu_{>98}Be_{<2}$ «window» plug) and from the other side by the already analyzed brass screw (Fig. 1, position *12* — brass screw). This sleeve was cut into two halves for SEM analysis. Figure 21 shows two SEM images for two different patches near the cut (*a*) and away from the cut (*b*) of this sleeve. In Table 16 the results of X-ray microanalysis are summarized over three analyzed patches.

As one can see, all the three analyzed patches are free from such chemical elements as Ti, Al, Si, K, Ca, Cl, Fe, Mg, found in the synthesized structure and on the surface of the Pd

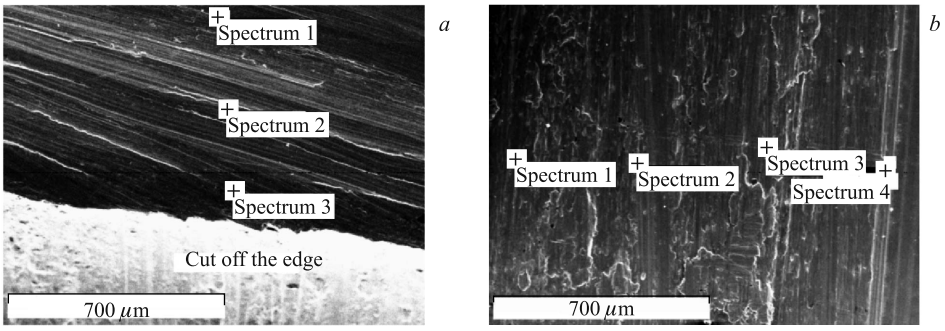

Fig. 21. SEM images of surface patches near the cut (*a*) and away from the split area of the brass sleeve (*b*)

specimen. Copper and zinc are observed practically in the same ratio and concentration as in the other measured brass specimen from which the brass screw is fabricated. Only presence of lead (Pb) and tantalum (Ta) remains unclear. However, we do not intend to deal with these elements further and explain their presence.

2.5. Structure and Element Composition of Window Plug from Beryllium Bronze (Fig. 1, Position *4* — $Cu_{>98}Be_{<2}$ «Window» Plug). Shown in Fig. 22 is a SEM image of a patch of window plug (thickness 2 mm and diameter 2 mm) from beryllium bronze ($Cu_{>98}Be_{<2}$). Table 16 provides element compositions measured by microelement analysis at the marked points (*a, b*) and unmarked ones (*c*) (see Table 16).

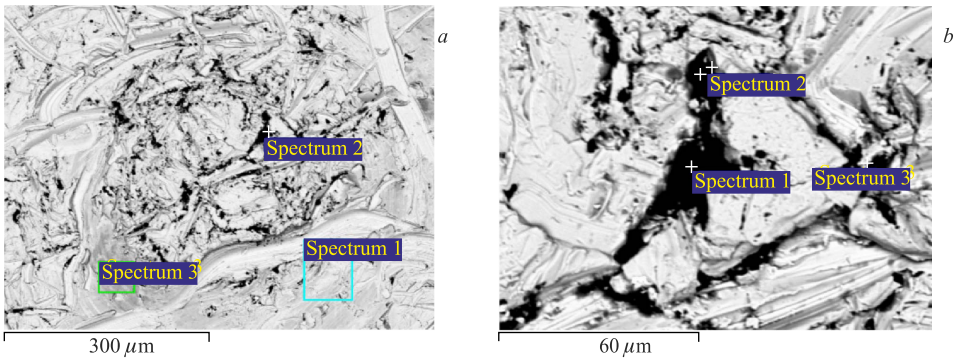

Fig. 22. Structure and element analysis of input beryllium bronze «window» plug

Table 16. **Element compositions on the surface patch at the points marked in Fig. 22**

Number	C	O	Al	Cl	Ca	Ti	Fe	Cu	Ag
Spectrum 1 (*a*)	7.5	5.18	—	—	—	—	—	87.32	—
Spectrum 3 (*a*)	13.63	16.95	0.37	—	—	—	0.41	68.65	—
Spectrum 1 (*b*)	20.33	42.94	30.92	—	0.29	0.36	—	4.54	0.62
Spectrum 2 (*b*)	13.96	41.44	41.49	—	—	0.55	—	2.55	—
Spectrum 3 (*b*)	4.46	44.89	45.75	—	—	0.4	—	4.5	—
Spectrum 1 (*c*)	6.87	22.18	0.75	0.49	—	—	—	69.7	—
Spectrum 2 (*c*)	6.17	2.72	0.43	—	—	—	—	88.55	2.14

As one can see from the table, the material that the window plug is composed of, beryllium bronze, is free from such impurities as Ti, Al, Si, K, Ca, Cl, Fe, Mg, which are observed in the synthesized structure and surface of the Pd specimen.

On the basis of the carried out studies into the surfaces of all the elements facing inside the HPC chamber, one can make the following *principal, experimentally substantiated and unambiguously proven conclusions [18]:*

1. The palladium specimen proved to be heavily deformed with a surface composed of cluster complexes of different chemical elements. The increase in the Pd volume is due to considerable disturbances of volume as formation of cracks and complexes based on different materials which takes place at processes of intense heating and subsequent cooling-recrystallization with precipitation of new phases. This phenomenon has nothing to do with the common swelling as a result of clusterization of Frenkel point defects.

2. In the Pd specimen surface facing the SNS synthesized structure there were observed considerable amounts of such chemical elements as C^{6}, O^{8}, Mg^{12}, Si^{14}, S^{16}, Cl^{17}, Ca^{20}, Ti^{22}, Fe^{26}, Cu^{29}, Zn^{30}, Pd^{46}.

3. In the cracks in the Pd specimen surface which had been penetrated by γ quanta, opposite to the first one, there were found such elements as C^{6}, O^{8}, V^{23}, Cr^{24}, Fe^{26}, W^{74}, Pb^{84}.

4. The following chemical elements were observed in the cracks on the side surface of the Pd specimen: C^{6}, O^{8}, V^{23}, Cr^{24}, Fe^{26}, W^{74}, Pb^{84}.

5. In the brass sleeve the following chemical elements were identified: C^{6}, O^{8}, Fe^{26}, Ta^{73}, Pb^{84} and, naturally, Cu^{29} and Zn^{30}.

6. In the surface of the SNS structure with dielectric properties and of light blue colour, which is generally typical of titanium compounds, there were found such elements as C^{6}, O^{8}, Mg^{12}, Al^{13}, Si^{14}, S^{16}, K^{19}, Ca^{20}, Ti^{22}, Cu^{29}, Zn^{30}, Pd^{46}. The discovered structure is shaped as «a volcano with a crater» of elliptic form with smooth and even walls in the middle.

On the crater floor, chiefly composed of titanium, there were discovered multiple plate-like formations with the following element composition: C^{6}, O^{8}, Mg^{12}, Al^{13}, Si^{14}, K^{19}, Ti^{22}, Cu^{29}, Zn^{30}. The titanium concentration found in the plate-like structures as rutile and its derivatives (TiO_2), as well as titanium deuterides like $Ti_{1.5}D_2$ or $Pd_{1.5}D_2$, reaches 66.42 wt. %. In other words, the titanium *concentration* is terribly great!

Apart from the plate-like formations, one can also find on the crater floor recrystallized brass polycrystals (Fig. 9, *a, b*), as well as ball-like structures and plate-like structures with palladium of $Pd_{1.5}D_2$ type (Fig. 10). Using the reflected electron registration method, these structures can be seen on the floor as light structures against the background of the dark floor and plate-like structures due to the large atomic number of palladium.

7. Considerable changes also occurred on the entrance plug from beryllium bronze, through which the flux of γ qaunta entered and which was placed on the axis of the HPC chamber. The central part of the plug has considerable changes on the surface as cracks and makes the impression of a structure which has been also exposed to high temperatures. On the dark patches (in studies by the reflected neutron method) one can observe a high concentration of aluminum (up to 45.75 wt. %) and a number of associated elements. Titanium and silver are also present in small quantities.

8. One should point out also the fact that the greatest changes in the chemical element compositions of the structures and presence of newly formed chemical elements take place where substantial changes in the surface structure are observed, i.e., in the cracks and fractures, in newly formed phases. In such a case, these macroscopic changes testify that the temperatures of the material in these places can be impressive.

9. At the same time, no other chemical elements were found on any of the investigated surface patches of the HPC initial elements apart from the inherent element compositions.

10. Therefore, the chemical elements observed a) on the surface of the central part of entrance window from beryllium bronze (Fig. 1, position *4* — $Cu_{0.98}Be_{0.02}$ «window» plug), b) on both the end and side surfaces of the Pd specimen (Fig. 1, position *9* — investigated specimen) and c) on the surface and inside the crater of the SNS structure and adjacent surface patches of the brass screw (Fig. 1, position *12* — brass screw) were produced under the action of γ radiation.

11. Irradiation by γ quanta of energy up to 23 MeV was carried out up to considerably higher fluences of γ quanta using three separate HPC chambers. The walls of all the HPC

chambers were fabricated from stainless steel, as opposed to the elements of the DHPC (see Fig. 1), i.e., in the absence of copper and zinc. As was in the first experiment, the HPC chambers were filled with dense gaseous deuterium under the pressure 3 kbar (one HPC chamber with pressure measurement) and 2 kbar (two HPC chambers) as well as specimens of V^{23}, Al^{13}, Cu^{29}, Pd^{46}, and Re^{75} as rods of different diameters (from 0.5 up to 2 mm) and of different lengths (from 1 up to 10 cm). The carried out SEM studies of the surface structure and microelement chemical analysis also allow one to confirm presence of nuclear reactions with considerable energy release and production of lighter elements leading to changes in the chemical composition of the irradiated specimens. As in the results described above, one observes the appearance of elements heavier than the materials forming the walls of all the elements of the DHPC chamber. It does not seem possible to make detailed research into the element composition of Pd (less activated) and Re specimens (more activated) due to their substantial activation. This concerns primarily specimens made of high-purity 99.98% Re^{75}. Such results are expected to be published later.

In the next article possible ways to explain the obtained anomalous effects and results will be discussed [18].

REFERENCES

1. *Subbotin M. L., Kurbatov D. K., Filimonova E. A.* Review of Studies of Demonstration Fusion Power Reactors // Issues of Atomic Science and Technology (VANT). 2010. Iss. 3, No. 8. P. 55–74.
2. *Chen F. F.* Introduction to Plasma Physics and Controlled Fusion. Second Ed. V. 1: Plasma Physics. Springer Science-Business Media, LLC, 2006. 425 p.
3. *Miyamoto K.* Plasma Physics for Nuclear Fusion. Revised Edition. Cambridge, Mass.: The MIT Press, 1989. 424 p.

3a. *Miyamoto K.* Principles of Plasma Physics and Controlled Fusion. M.: Fizmatlit, 2007. 424 p. (in Russian).

4. *Ishkhanov B. A., Kapitonov I. M.* Electromagnetic Interaction with Atomic Nuclei. M.: MSU, 1979. 215 p.
5. *Hulten L., Sugawara M.* Two-Nucleon Interaction Problem // Structure of Atomic Nucleus. M.: For. Lit. Publ., 1959. P. 22.

6a. *Bethe H., Morisson P.* Elementary Nuclear Theory. N. Y.: John Willey & Sons, Inc.; London; Chapman & Hall, Limited, 1956. 356 p.

6b. *Bethe H. A., Peirls R. E.* Quantum Theory of the Diplon // Proc. Roy. Soc. A. 1935. V. 148. P. 146–156.

7. *Wiśniewski R.* High Pressure Apparatus for Gaseous Hydrogen up to 25 kilobars and Temperature Range $-50\,^{\circ}\mathrm{C} - +100\,^{\circ}\mathrm{C}$ // Rev. Sci. Instr. 1970. V. 41, No. 3. P. 455–464.
8. *Wiśniewski R., Didyk A. Yu., Wilczynska-Kitowska T.* Russian Federation Patent. 2012 (in press).
9. *Mukhin K. N.* Experimental Nuclear Physics. V. 1: Physics of Atomic Nucleus. M.: Energoatomizdat, 1983. 616 p.
10. *Ishkhanov B. S. et al.* Cross Sections of Photon Absorption by Atomic Nuclei with Nucleon Number 12–65. Preprint of MSU SINP 2002-27/711. M.: MSU, 2002. P. 22.
11. *Belov A. G. et al.* MT-22 Microtron. JINR Commun. P9-82-301. Dubna, 1982.
12. Metal Hydrides / Editors and major contributors: W. M. Mueller, J. P. Blackledge, G. G. Libowitz. N. Y.; London: Acad. Press, 1968. P. 63.

13. *Didyk A. Yu., Wiśniewski R., Altynov V. A.* Extrapolations of Hydrogen Molar Volumes by Virial Expansion Series in Wide Temperature and Pressure Intervals. JINR Commun. E17-2008-183. Dubna, 2008.
14. *Buchnev V. N., Komochkov M. M., Mokrov Yu. V.* Energy Dependences of Sensitivity of Some Neutron Dosimeters in the Energy Range from 1 eV to 4 keV. JINR Commun. P16-85-802. Dubna, 1985.
15. *Zhuchko V. E., Zen Chan Uk.* Polynomial Representation of Thick-Target Bremsstrahlung Spectra for Electrons of Energy 10–22 MeV // At. Energy. 1985. V. 59, Iss. 1. P. 65–66 (in Russian).
16. *Tarasko M. Z., Soldatov A. S., Rudnikov V. E.* Description of Thick-Target Bremsstrahlung Spectra for Electrons of Energy 4–12 MeV // At. Energy. 1988. V. 65, Iss. 4. P. 290–291 (in Russian).
17. Experimental Nuclear Physics. V. 1 / Ed. E. Segre. N. Y.; London, 1953. 616 p.; M.: For. Lit. Publ., 1955. 662 p.
18. *Didyk A. Yu., Wisniewski R.* Nuclear Reactions in Gaseous Deuterium under High Pressure and in Saturated with Deuterium Palladium, Induced by γ-Quanta // Lett. J. Exploring the Frontiers of Phys. 2012. V. 99. P. 22001–22006.

Received on April 4, 2012.